Cancer Immunology, Immunotherapy (2025) 74:116
https://doi.org/10.1007/s00262-024-03883-3

RESEARCH

Comprehensive analysis and experimental validation of disulfidptosis-associated prognostic signature and immune microenvironment characterization of gastric cancer

Huangjie Zhang[2] · Jinguo Hu[3] · Yuanqiang Li[2] · Yanyang Liu[4] · Huize Shen[1] · Zeng Wang[2] · Qinglin Li[4]

Received: 29 September 2024 / Accepted: 3 November 2024 / Published online: 25 February 2025

Abstract

Background Gastric cancer (GC) is one of the most common causes of cancer-related death worldwide. As a novel form of programmed cell death, disulfidptosis is characterized by excessive cysteine accumulation, disulfide stress and actin destruction. There is evidence that targeting disulfidptosis is a promising anticancer strategy. Further improvement of GC risk stratification based on disulfidptosis has positive clinical significance.

Methods We analyzed the expression levels of disulfidptosis-associated genes (DPAGs) in normal and GC tissues and characterized the molecular subtypes of GC patients. Based on the characteristics of DPAG subtypes, differentially expressed prognosis-related genes were selected by LASSO-univariate Cox analysis and multivariate Cox analysis analyzed to establish a prognostic model. Using single-cell sequencing analysis reveals the cell subpopulation for GC. The function of the selected target in GC was verified by in vitro experimental means, including siRNA, qRT-PCR, Western blot, CCK-8, and Transwell assay.

Results DPAG score was verified to be an independent prognostic factor of GC and was significantly associated with poor prognosis of gastric cancer. Subsequent studies on subgroup immunoinfiltration characteristics, drug sensitivity analysis, immunotherapy response and somatic mutation characteristics of DPAG score comprehensively confirmed the potential guiding significance of DPAG score for individualized treatment of gastric cancer patients. Single-cell sequencing analysis revealed the expression characteristics of DPAG-related prognostic signatures across cell subpopulations. In vitro experiments showed APC11, as one of the selected DPAGs, was highly expressed in gastric cancer, and knockdown of APC11 could significantly inhibit the proliferation and migration of GC cells, demonstrating the reliability of bioinformatics results.

Conclusion The results of this study provide a new perspective for exploring the role of disulfidptosis in the occurrence and development of GC.

Keywords Disulfidptosis · Gastric cancer · Single-cell sequencing analysis · Prognostic model · Immune filtration characterization · APC11

Introduction

According to GLOBOCAN 2020, gastric cancer (GC) accounts for 7.7% of all cancer deaths, making it one of the most common cancer-related causes of death in the world

Authors Huangjie Zhang, Jinguo Hu, Yanyang Liu, Huize Shen contributed equally to this work

✉ Zeng Wang
wangzeng@zjcc.org.cn

✉ Qinglin Li
qinglin200886@126.com

[1] School of Pharmaceutical Sciences, Zhejiang Chinese Medical University, Hangzhou, Zhejiang, China

[2] Zhejiang Cancer Hospital, Hangzhou, Zhejiang, China

[3] Hangzhou TCM Hospital Affiliated to Zhejiang Chinese Medical University, Hangzhou, Zhejiang, China

[4] Postgraduate training base Alliance of Wenzhou Medical University (Zhejiang Cancer Hospital), Hangzhou, Zhejiang, China

[1]. Despite a decline in GC mortality in recent decades due to early detection and advances in chemotherapy and targeted therapies, the 5-year survival rate is still only 32% [2]. With the progress of cancer biomarker identification and targeted monitoring, the value of GC risk stratification based on patient prognosis for GC patient management and treatment guidance has received more and more attention [3, 4]. Further improvement of GC risk stratification has positive clinical significance.

Recently, a novel form of programmed cell death characterized by excessive disulfide formation in the actin cytoskeleton and breakdown of actin filaments, called disulfidptosis, has been reported as a promising anticancer strategy [5]. During disulfidptosis activation, high expression of SLC7A11 leads to increased extracellular cysteine uptake, which leads to excessive accumulation of intracellular cysteine, ultimately leading to disulfide stress in cell metabolism and destruction of actin structure [6, 7]. In addition, the process requires the production of a reduced form of nicotinamide adenine dinucleotide phosphate (NADPH) by the pentose phosphate pathway (PPP) under starvation conditions [5]. However, the role of disulfidptosis in GC remains unknown.

There are clues to the role of disulfidptosis in GC. As a key molecule of disulfidptosis, SLC7A11 expression levels determine the different responses of cancer cells to oxidative stress [8]. In GC, SLC7A11 has been reported to be involved in inducing programmed death processes [9, 10]. In the process of GC development, the specific region of SLC7A11 mRNA 3 '-UTR increases the level of L-glutathione (GSH) and inhibits the production of reactive oxygen species (ROS) in GC cells through interaction with lncRNA ELAVL1. Ultimately, GC cells are protected from programmed cell death and distant metastasis occurs [11]. In addition, stemness of GC is also associated with the signaling pathway involved in SLC7A11 [12]. In GC patients, the expression level of microsatellite instability (MSI), tumor mutation burden (TMB), and neoantigens are all prognostic indicators reflecting antigens of immunotherapy response [13–15]. In a pan-cancer study, STAD was the only cancer type in which TMB, MSI, and neoantigens were all significantly positively associated with SLC7A11 expression [16]. This study highlights the potential value of disulfidptosis in GC while revealing the importance of GC immunotherapy.

The tumor microenvironment (TME) plays a critical role in tumor invasion and metastasis [17]. Many evidences indicate that the influence of TME is one of the key reasons for the complexity and poor prognosis of GC [18, 19]. Fully understanding the tumor immune microenvironment and studying the effects of TME components on cancer will help reveal new prognostic factors and potential therapeutic targets for GC [20–22].

In this study, we analyzed the expression levels of disulfidptosis-associated genes (DPAGs) in normal and GC tissues and characterized GC molecular subtypes. Based on the characteristics of DPAG subtypes, a prognostic model was established after analysis of differentially expressed genes related to prognosis, and it was verified that DPAG score is an independent prognostic factor of GC and is significantly correlated with poor prognosis of gastric cancer. In vitro experiments showed APC11, as one of the selected DPAGs, was highly expressed in gastric cancer, and knockdown of APC11 could significantly inhibit the proliferation and migration of GC cells, demonstrating the reliability of bioinformatics results. The results of this study provide a new perspective for the involvement of disulfidptosis in the occurrence and development of GC.

Materials and methods

Transcriptome matrix download and preprocessing

In this study, we obtained transcriptome matrices and clinical information from the TCGA and GEO databases using the keyword "gastric cancer". A total of 402 GC samples, including 31 normal samples and 371 GC samples, with complete clinical information were collected from a publicly available TCGA database. From the GEO database, we downloaded the GSE84437 dataset that included 433 GC samples (Supplementary Table 1). The TCGA gene symbols were matched and annotated based on Ensembl's human genome browser GRCh38.p13 using the Perl programming language environment, while the gene annotation for GSE84437 was based on platform file GPL6947. We standardized and removed batch effects from the TCGA-GC and GEO-GC matrix data using the "limma" and "sva" scripts [23].

Identification of molecular subtypes of disulfidptosis-associated gene (DPAG) in GC

In accordance with prior research, we have gathered a list of 16 genes associated with disulfidptosis (DPAGs) for further analysis (Supplementary Table 2) [24]. Employing the "ConsensusClusterPlus" script, we have classified GC samples into distinct molecular subtypes based on the expression profiles of these 16 DPAGs, utilizing the optimal classification method. The "survival" script and the log-rank algorithm were utilized to investigate clinical survival outcomes among different DPAG molecular subtypes in GC samples. Furthermore, unsupervised principal component analysis (PCA) was conducted through

the "ggplot2" script to assess the distributional characteristics of various DPAG molecular subtypes in GC samples. Finally, the "GSVA" algorithm was employed to compute significant variations in KEGG signaling pathways between different DPAG molecular subtypes, utilizing the KEGG reference gene set "c2.cp.kegg.v7.2.symbols".

Identification of differentially expressed genes (DEGs) among DPAG molecular subtypes and consensus clustering analysis

Firstly, we applied the "limma" script to identify differentially expressed genes (DEGs) between different DPAG molecular subtypes, using a *p*-value cutoff of less than 0.05. Next, based on the DEGs identified, we conducted consensus clustering analysis of GC samples using the "ConsensusClusterPlus" script, which resulted in the classification of samples into different gene subtypes. Additionally, we utilized the "clusterProfile" script to perform KEGG and GO pathway annotation of the DEGs between different DPAG molecular subtypes.

Immune microenvironment characterization and immunotherapy response prediction

We employed the "estimate" and "limma" scripts on the transcriptional matrix of TCGA-GC and GEO-GC samples to derive the immune status of each GC sample, comprising of immune, stromal, and estimate scores, and tumor purity. Furthermore, by leveraging the marker genes specific to 23 immune cell types, we utilized the "GSVA" algorithm to quantify the abundance of immune cells in GC samples. Additionally, we retrieved the immune therapy response data for CTLA4 and PD1 in GC samples from The Cancer Immunome Atlas (TCIA) database.

Calculation of DPAG score and prognostic model construction

In this study, we conducted an integrated analysis of DEGs between different DPAG molecular subtypes and survival information data from GC samples. We employed the "survminer" script to calculate the hazard ratio (HR) and P values of DEGs, and the LASSO-univariate Cox analysis based on the "glmnet" script to screen for prognostic factors related to GC prognosis. To further screen for prognostic factors with independent prognostic value, we performed multivariate Cox analysis and calculated the DPAG score of each independent prognostic factor based on its coefficient and expression profile, using the formula: DPAG score = (Risk coefficient$_1$ * Factor A$_1$) + (Risk coefficient$_2$ * Factor A$_2$) + … + (Risk coefficient$_n$ * Factor A$_n$). We determined the optimal cutoff value of the DPAG score and classified the GC samples into low- and high-DPAG-score subgroups. We randomly divided the GC samples into training and validation sets in a 6:4 ratio, using the "caret" script, and evaluated the clinical prognosis outcomes between the DPAG score subgroups with the "survival" script. Moreover, we employed the "ggalluvial" package to explore the potential associations between DPAG subtypes, gene subtypes, DPAG score, and clinical survival outcomes.

Independent prognostic analysis and nomogram model development

We systematically integrated clinical information from GC samples obtained from the TCGA and GEO databases, and employed both univariate and multivariate Cox analysis to evaluate the HR and P values of different clinical features and DPAG scores. The independence of DPAG scores was also assessed. To further evaluate the predictive performance of DPAG scores, we utilized the "survivalROC" package to assess the area under the curve (AUC) of survival for GC samples at 1 year, 3 years, and 5 years. Moreover, we developed a nomogram using the "rms" and "regplot" scripts based on clinical information and DPAG scores to predict the prognosis of 1-year, 3-year, and 5-year survival probabilities. To assess the accuracy of the nomogram, we utilized calibration curves to validate the consistency between the predicted and actual survival probabilities. Additionally, we calculated the concordance index (C-index) of DPAG scores and each clinical variable based on the "pec" and "rms" scripts.

Chemotherapy drug prediction and somatic mutation characterization

We utilized the Genomics of Drug Sensitivity in Cancer (GDSC) database to investigate potential chemotherapy drugs that might exhibit varying efficacy between the different DPAG score subgroups, utilizing the "pRRophetic" script. Moreover, we downloaded somatic mutation data (MAF) from the TCGA database and preprocessed it using a Perl script, with subsequent analysis of the mutation landscape characteristics of the DPAG score subgroups undertaken using the "maftools" script.

Preprocessing and analysis of single-cell sequencing data

In this study, we utilized the single-cell RNA sequencing dataset GSE163558 from the GEO database, which contains tumor tissue samples from three gastric cancer patients. The raw data were preprocessed using the Seurat R package

(v4.0.5). Quality control was performed based on gene expression levels for each cell, filtering out cells with fewer than 200 or more than 6000 genes, and those with more than 15% mitochondrial gene content. Subsequently, gene expression data were normalized using standard methods, and highly variable genes were selected through the "Find Variable Features" function to retain key biological information in the data. After quality control, data from different samples were integrated to eliminate batch effects. The integration process was conducted using the "Find Integration Anchors" and "Integrate Data" functions. Principal component analysis (PCA) was then applied for linear dimensionality reduction, with the top 20 principal components selected for downstream analyses. Additionally, nonlinear dimensionality reduction was performed using t-SNE (t-distributed Stochastic Neighbor Embedding) and UMAP (Uniform Manifold Approximation and Projection) algorithms to visualize cell clustering results. Cell subpopulations were identified by clustering in PCA space using the "Find Clusters" function, with a resolution of 0.8. Each cell population was annotated by comparing them to known gastric cancer marker genes, and the "Single"R" method was employed to assist with cell type annotation, further improving the accuracy of cell group definitions. To explore differentially expressed genes among cell subpopulations, the "Find Markers" function was used. Genes with a p-value < 0.05 and log2 fold change > 0.25 were considered significantly differentially expressed. UMAP plots were used to visualize the spatial distribution of target gene expression across different cell subpopulations.

Cell culture and transfection

The human normal gastric mucosal epithelial cell line GSE-1, as well as the human gastric cancer cell lines MGC803, MKN45, and AZ521, were all purchased from the Cancer Institute of the Chinese Academy of Medical Sciences (Beijing, China). The cells were cultured in DMEM medium supplemented with 10% fetal bovine serum and 100 U/mL penicillin–streptomycin under conditions of 37 °C and 5% CO_2. To knock down APC11 in these cells, siRNAs targeting APC11 were purchased from RiboBio (Guangzhou, China) and transfected into the cells using Lipofectamine 3000 (Invitrogen, USA). Subsequent experiments were conducted 48 h post-transfection.

RNA extraction and qRT-PCR

Total RNA from cells and tissues was extracted using TRIZOL (Catalog No. 15596026, Invitrogen). For reverse transcription, a reverse transcription kit (F0202O, LABLEAD) was used. Briefly, 3 μg of total RNA was added to a PCR tube along with reverse transcription premix, Oligo(dT)20VN, and Random Hexamers. The mixture was then incubated at 55 °C for 30 min followed by 5 min at 85 °C to obtain cDNA. The expression of APC11 was detected by qRT-PCR using SYBR Green dye, with the following primers: h-APC11-F: ATTAGGTTGGCGAAGGCTCTG and h-APC11-R: GTT GATGGGCACCTGTGGAT. β-actin was used as an internal control with the following primers: h-β-actin-F: GGCATC GTCACCAACTGGGAC and h-β-actin-R: CGATTTCCC GCTCGGCCGTGG. The qRT-PCR reactions were carried out using a qRT-PCR kit (R0202, LABLEAD) according to the manufacturer's instructions.

Protein extraction and western blot

For cell protein extraction, after discarding the cell culture supernatant, cells were washed twice with pre-chilled PBS. A total of 100 μL RIPA lysis buffer (Catalog No. PC101, Epizyme) was added, and cells were scraped off with a cell scraper and transferred to a 1.5 mL centrifuge tube. The tube was incubated on ice for 30 min. Following this, the sample was centrifuged at 13,000 rpm for 15 min at 4 °C, and the supernatant was transferred to a new 1.5 mL centrifuge tube. Protein concentration was determined using a BCA protein assay kit (Catalog No. P0009, Beyotime). For Western blot analysis, 30 μg of protein was separated by 10% polyacrylamide gel electrophoresis and transferred to a 0.22 μm PVDF membrane. The membrane was blocked with 5% non-fat milk at room temperature for 1 h and then incubated overnight at 4 °C with primary antibodies against APC11 (Catalog No. SC-517142, 1:500, Santa Cruz) and β-actin (Catalog No. AC026, 1:10,000, Abclonal). The PVDF membrane was then incubated with an HRP-conjugated secondary antibody (1,721,019, 1:2000, Bio-Rad) at room temperature for 1 h. The protein bands were visualized using an enhanced ECL chemiluminescence detection kit (Catalog No. E411, Vazyme) and imaged with a gel imaging system (Amersham ImageQuant 800, Cytiva).

Immunofluorescence staining

Cells were seeded on cell slides (Catalog No. YA0350, Solarbio) placed in a 24-well plate. After 24 h, the cells were washed with PBS and fixed with 10% formalin fixative solution (Catalog No. BL401A, Biosharp) at room temperature for 20 min. The cells were then washed three times with PBS and blocked with blocking solution (5% goat serum) for 1 h. After blocking, APC11 antibody (1:200) was added, and the cells were incubated overnight at 4 °C. The following day, the cells were incubated with a fluorescently labeled secondary antibody (1:500, RGAM004, Proteintech) at room temperature for 2 h in the dark. After washing the cells three times with PBS, an anti-fade mounting medium (Catalog No. ab188804, Abcam) was used to mount the slides. Images

were captured using a laser confocal microscope (RHD25, NIKON).

CCK-8 assay and colony formation assay

Cells were seeded in a 96-well plate at a density of 6,000 cells per well. Every 24 h, 10 uL of CCK-8 reagent (Catalog No. A311, Vazyme) was added to each well, followed by incubation at 37 °C for 2 h. The absorbance at 450 nm was then measured using a microplate reader. Cells were seeded in a 6-well plate at a density of 1000 cells per well. Once the cells formed visible colonies, they were fixed with 10% formalin fixative solution at room temperature for 20 min. The cells were then stained with 0.1% crystal violet staining solution (Catalog No. C0121, Beyotime) at room temperature for 30 min. After washing with deionized water and air drying, the colonies were photographed.

Cell migration assay

A total of 10,000 cells were seeded into 12 mm cell culture inserts with serum-free DMEM medium, while the lower chamber was filled with DMEM medium containing 10% FBS. After 48 h, the cells were fixed with 10% formalin fixative solution at room temperature for 20 min. The cells were then stained with 0.1% crystal violet staining solution (Catalog No. C0121, Beyotime) at room temperature for 30 min. After washing with deionized water and air drying, images were captured using a fluorescence inverted microscope (IX83, Carl Zeiss).

Statistical analysis

All data processing and analysis in this study were conducted using the R software (R × 64 4.1.0), GraphPad Prism 9.0 and Perl language environment. The Spearman correlation algorithm was employed to determine the correlation between DPAG score and the immune microenvironment. The Wilcoxon test was utilized to compare two groups, while ANOVA was employed for multiple groups. A p-value of less than 0.05 was considered statistically significant.

Results

In order to investigate the potential role of disulfidptosis-associated genes (DPAGs) in the development of GC, we collected a set of 16 DPAGs for analysis. Using the "limma" script, we conducted an expression analysis of these DPAGs in both normal and GC tissues. Based on differential expression analysis, we found 12 DPAGs to be significantly differentially expressed between these two groups, with all 12 DPAGs showing significantly higher expression levels in the GC group compared to normal tissues (Fig. 1A). Protein–protein interaction network (PPI) diagram revealing the potential interactions between the 16 DPAGs (Fig. 1B). Our CNV mapping results revealed that a majority of the DPAGs exhibited CNV amplification in GC samples, including TLN1, SLC3A2, ACTB, and FLNA, while RPN1 and LRPPRC showed CNV deletion (Fig. 1C). Furthermore, our mutation characterizations analysis revealed the mutation profile of these DPAGs, with SLC3A2, MYH9, FLNB, and FLNA exhibiting higher mutation frequencies of 7%, 7%, 6%, and 6%, respectively (Fig. 1D). Overall, these findings suggest that DPAGs may play an important role in the development of GC, and further investigations are warranted to explore their potential as diagnostic or therapeutic targets.

Molecular subtype characteristic exploration based on DPAGs for GC

In the subsequent investigation, we delved further into the molecular subtype characteristics of GC by analyzing the expression profiles of 16 DPAGs. Our univariate Cox analysis results revealed that five DPAGs were closely associated with the prognosis of GC. Specifically, FLNA and TLN1 were identified as risk prognostic factors, while OXSM, NDUFS1, and LRPPRC were favorable prognostic factors (Fig. 2A). Based on unsupervised consensus clustering analysis, we successfully classified 804 GC samples into three independent molecular subtypes (k = 3), where subtype A had 478 samples, subtype B had 205 samples, and subtype C had 121 samples. Moreover, clinical survival outcome analysis uncovered significant differences in the survival prognosis of GC samples among the three independent molecular subtypes, where subtype C showed poorer clinical survival outcome than subtypes A and B (Fig. 2B, $p = 0.012$). Additionally, an unsupervised PCA plot based on DPAGs clearly distinguished the distribution patterns of different molecular subtypes of GC, further confirming the independence of the three molecular subtypes (Fig. 2C). Further analysis of the expression profiles of the 16 DPAGs in GC samples based on clinical features and survival status revealed significant differences in the expression of DPAGs among the molecular subtypes of GC (Fig. 2D). Using the GSVA algorithm, we also evaluated the potential regulatory mechanisms in different molecular subtypes of GC. Compared with DPAGs subtype A, we observed that metabolism related signaling pathways such as pyrimidine metabolism and glyoxylate and dicarboxylate metabolism were significantly upregulated in DPAGs subtype B. Notably, compared with DPAGs subtype B, we found that cell cycle related signaling pathways were significantly downregulated in DPAGs subtype C (Fig. 2E and F).Our results confirm that DPAGs can accurately distinguish different molecular subtypes of GC and are closely associated with the prognosis of GC.

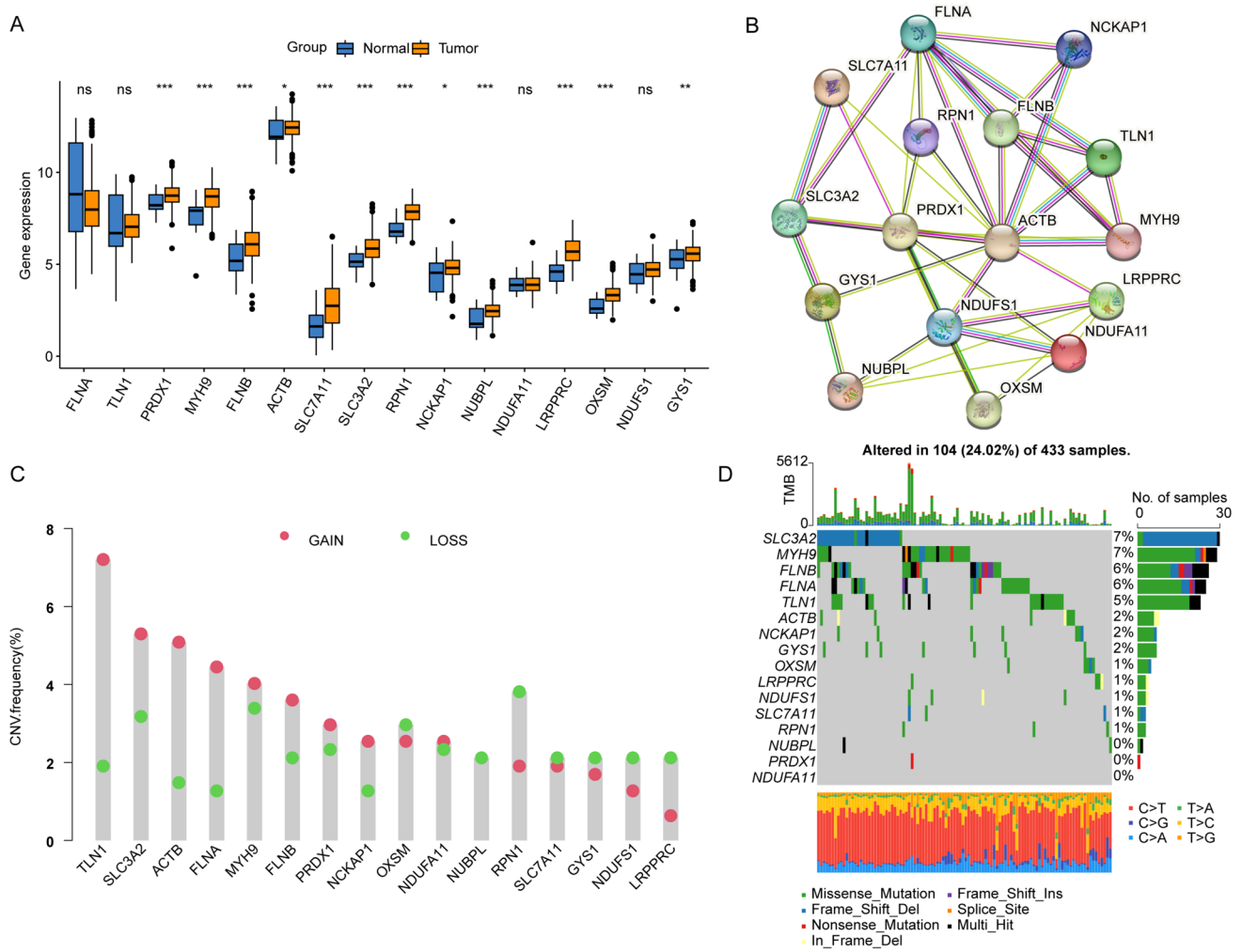

Fig. 1 Potential functional analysis of DPAGs in GC. (**A**) Differential expression analysis of the 16 DPAGs in the normal and GC groups. (**B**) PPI network diagram revealing the potential interactions between the 16 DPAGs. (**C**) CNV characteristics of DPAGs in GC. (**D**) Mutation frequency characteristics of DPAGs. $*p<0.05$, $**p<0.01$, $***p<0.001$, ns, no significance

Immune microenvironment characteristic of different DPAG subtypes

We conducted a comprehensive analysis to assess the immunotherapy response and immune infiltration features of GC samples in different DPAG subtypes using an immune evaluation algorithm. We utilized the TCIA database to evaluate the immunotherapy response to CTLA4 and PD1 in GC across each DPAG subtype. Our IPS results revealed that GC samples in DPAG subtype A exhibited high sensitivity to CTLA4 and PD1 treatment, suggesting that these samples may have a favorable response to immunotherapy (Fig. 3A–D). Furthermore, we employed the ESTIMATE algorithm to evaluate the immune status of GC samples in different DPAG subtypes. Our results indicated a significant decrease in stromal, immune, and ESTIMATE scores and an increase in tumor purity in DPAG subtype B, which had a better survival prognosis (Fig. 3E). Moreover, we utilized the ssGSEA algorithm to investigate the immune infiltration status of GC samples across DPAG subtypes. Our findings demonstrated significant variations in the immune infiltration status of GC samples, with activated B cells, eosinophil, macrophage, and mast cells being considerably reduced in DPAG subtype B (Fig. 3F). Overall, our results suggest that the molecular subtypes based on DPAG can effectively predict the immunotherapeutic response of GC and correlate with the immune infiltration status, which may have implications for personalized immunotherapy in GC patients.

Exploration of DPAG subtype-associated genes molecular subtypes for GC

To better understand the potential molecular mechanisms between different DPAG subtypes, we used the "limma"

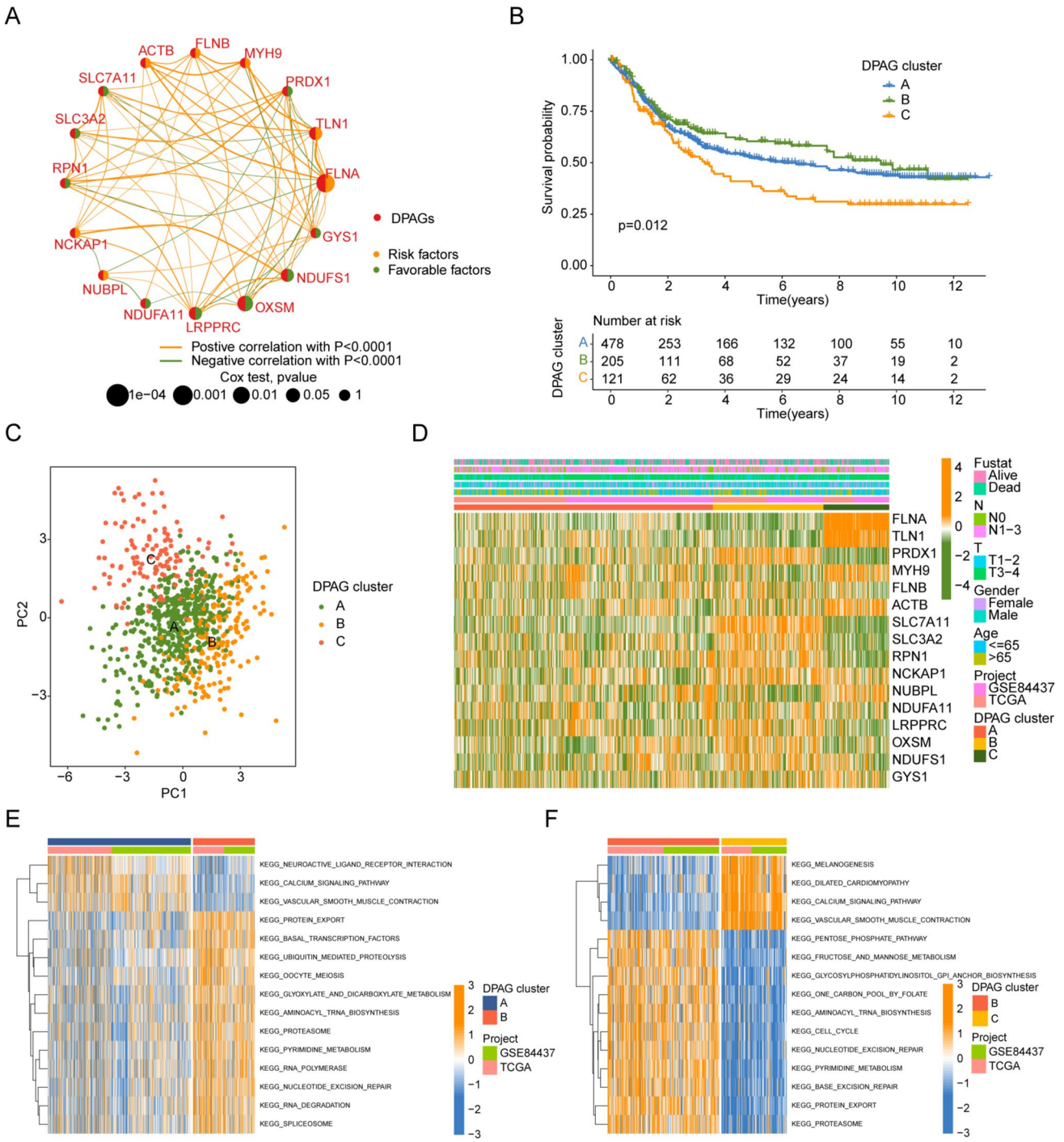

Fig. 2 Identification of molecular subtypes based on DPAGs in GC. (**A**) The network shows the correlation and prognostic value of DPAGs. (**B**) Clinical survival prognosis analysis of GC in different DPAG subtypes. (**C**) The unsupervised PCA plot exhibits the different patterns of GC samples in DPAGs subtypes. (**D**) The expression profile of DPAGs in different DPAG subtypes and clinical characteristics. (**E**, **F**) GSVA reveals the significantly different KEGG signaling pathway between DPAG subtypes

script to calculate differentially expressed genes (DEGs) between three independent DPAG analysis subtypes. Under the filtering threshold set at $p < 0.05$, we collected a total of 1958 DEGs to explore the molecular mechanisms between different DPAG subtypes. Based on the expression profiles of these DEGs, we performed unsupervised consensus clustering analysis on GC samples, and the results showed that when k = 3, the classification had the optimal stability, with 337 samples in gene subtype A, 321 samples in gene subtype B, and 146 samples in gene subtype C (Fig. 4A). Clinical

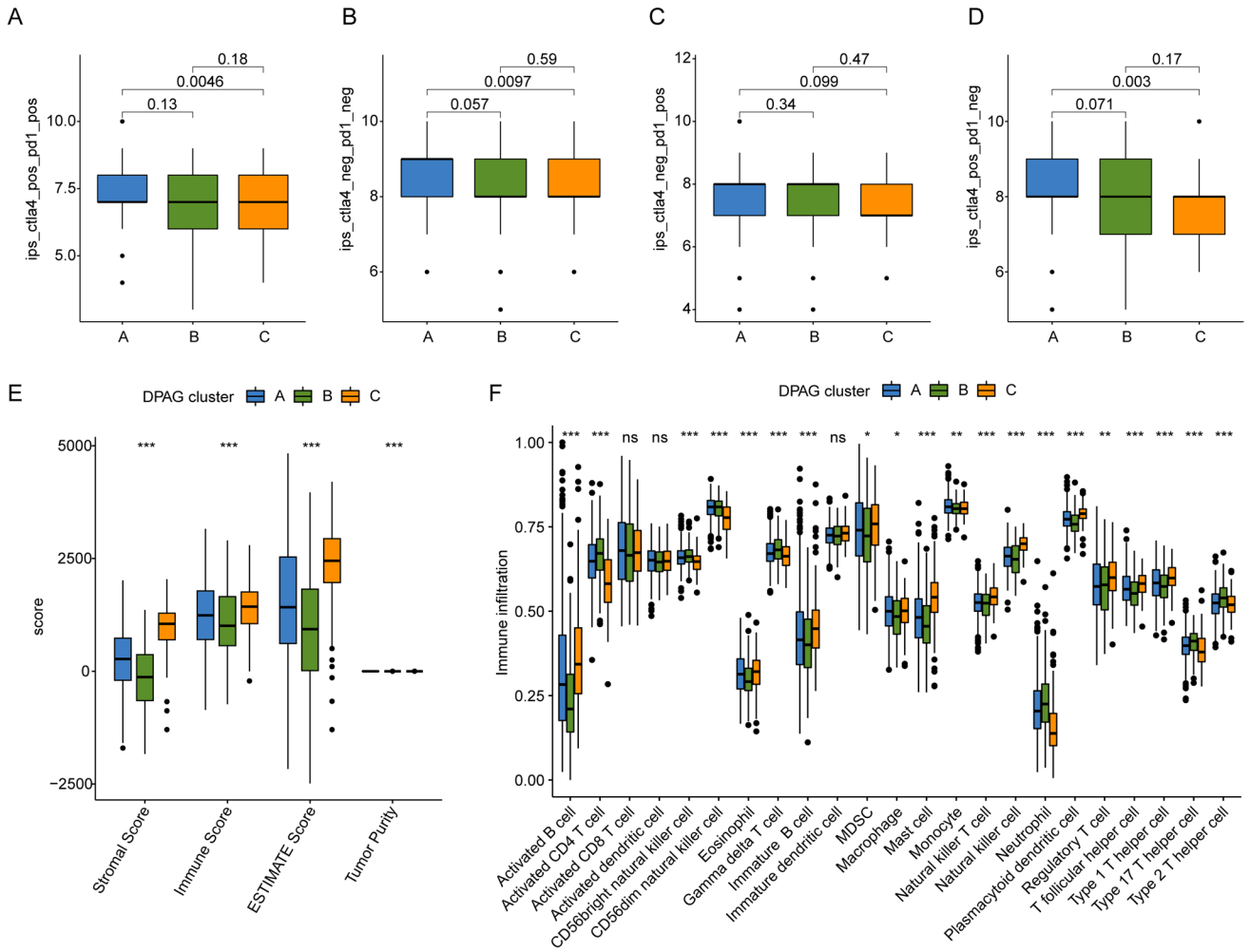

Fig. 3 Immune microenvironment analysis of GC samples in different DPAG subtypes. (**A**–**D**) IPS results reveal immunotherapeutic response of DPAG molecular subtypes to CTLA4 and PD1. (**E**) Immune status assessment. (**F**) The fraction of 23 immune cells in different DPAG subtypes via ssGSEA algorithm. $*p<0.05$, $**p<0.01$, $***p<0.001$, ns, no significance

survival curve analysis showed that the prognosis of GC samples in gene subtype B was significantly better than that in gene subtypes A and C (Fig. 4B, $p<0.001$). In addition, we found that the expression of DPAGs differed significantly among different gene subtypes. In gene subtype C, we observed significantly high expression of FLNA, TLN1, MYH9, ACTB, NUBPL, and NDUFA11, while PRDX1, FLNB, SLC7A11, SLC3A2, RPN1, LRPPRC, OXSM, NDUFS1, and GYS1 were significantly downregulated in gene subtype C (Fig. 4C). KEGG enrichment analysis results showed that DEGs were significantly associated with cell cycle, biosynthesis of cofactors, DNA replication, and the p53 signaling pathway (Fig. 4D). GO analysis results showed that DEGs were significantly enriched in biological processes such as extracellular matrix organization, collagen-containing extracellular matrix, and extracellular matrix structural constituents (Fig. 4E).

Development of a prognostic model based on DPAG subtype-associated DEGs

To evaluate the potential prognostic value of DPAG subtype-associated DEGs in GC, we calculated the DPAG scores of GC samples based on univariate and multivariate Cox analysis, and developed a novel prognostic model. Based on LASSO-univariate Cox analysis, we obtained 26 feature variables associated with GC prognosis. Using multivariate Cox analysis, we identified 19 independent prognostic factors associated with GC prognosis and calculated the DPAG score for each GC sample. Based on the prognostic characteristics of DEGs, we randomly divided GC samples into a training set (n = 563) and a validation set (n = 241) at a ratio of 6:4. In the entire set, GC samples were divided into low- and high-DPAG-score subgroups according to the optimal cutoff value of DPAG score. The scatter plot results indicated that most of the deceased samples in the

GC samples were more inclined to the high-DPAG-score subgroup (Fig. 5A). Clinical prognostic outcome results showed that the OS rate of GC samples in the low-DPAG-score subgroup was significantly better than that in the high-DPAG-score subgroup (Fig. 5B, $p < 0.001$). The unsupervised PCA plot showed that the prognostic features based on DPAGs could accurately distinguish between the low- and high-DPAG-score subgroups (Fig. 5C). It is worth noting that in the DPAG subgroups, the DPAG score of subgroup C with the worst clinical prognosis was significantly higher than that of subgroups A and B (Fig. 5D). In the gene subtypes, the DPAG score of the subgroup C with the worst clinical survival outcome was also significantly higher than that of subgroups A and B (Fig. 5E). The Sankey diagram showed the association between clinical survival outcomes of GC samples and DPAG subtype, gene subtype, and DPAG score, indicating that GC samples in the DPAG and gene subtypes with poor prognosis were more likely to be in the high-DPAG-score subgroup, and significantly correlated with poor prognosis (Fig. 5F). Based on these results, we speculate that a prognostic model based on DPAG-related DEGs can accurately evaluate the survival outcome of GC samples.

Construction of a nomogram model based on DPAG score and clinicopathological characteristics

We developed a nomogram integrating clinicopathological features of GC samples with DPAG score to accurately evaluate the 1-, 3-, and 5-year survival probabilities. We found that the nomogram constructed with DPAG score and different clinicopathological features could accurately assess the survival probabilities of GC samples in the entire set (Fig. 6A and B). The C-index curve results indicated that the C-index of DPAG score was significantly higher than age, gender, T, and N, suggesting that DPAG score predicted the clinical prognosis and survival ability of GC samples better than other clinicopathological features (Fig. 6C). In the training and validation sets, we found that the predicted 1-, 3-, and 5-year OS rates based on the nomogram were consistent with the actual OS rates, and the C-index curve showed that the C-index of DPAG score was significantly higher than other clinicopathological features in the training and validation sets (Fig. 6D–I). Overall, our results suggest that the nomogram based on DPAG score and clinicopathological features can accurately predict the 1-, 3-, and 5-year survival probabilities of GC samples, and the predictive ability of DPAG score is significantly better than that of clinical features of GC.

Independent prognosis analysis of DPAG score in GC

Based on univariate and multivariate Cox analysis, we further evaluated the independence of the DPAG score as a prognostic factor for GC in the entire, training, and validation sets. In the entire set, both univariate and multivariate Cox regression analysis showed that age ($HR > 1$, $p < 0.001$), T stage ($HR > 1$, $p < 0.05$), N stage ($HR > 1$, $p < 0.001$), and DPAG score ($HR > 1$, $p < 0.001$) were significantly associated with poor prognosis of GC (Fig. 7A). Similarly, in the training and validation sets, both univariate and multivariate Cox regression analysis demonstrated that the DPAG score was an independent prognostic factor for GC, indicating that the DPAG score was not confounded by other clinical variables (Fig. 7B and C). Time-dependent ROC curves showed that the AUCs for 1-, 3-, and 5-year survival in the entire set were 0.678, 0.701, and 0.711, respectively; in the training set were 0.681, 0.712, and 0.734, respectively; and in the validation set were 0.667, 0.678, and 0.661, respectively (Fig. 7D–F). Based on these findings, we conclude that the DPAG score is an independent prognostic factor for GC and is significantly associated with poor prognosis of GC.

Development of prognosis model based on DPAG score in the training and validation sets

To further clarify the accuracy and reliability of the prognostic model based on DPAG score in predicting the clinical prognosis of GC, we constructed a prognostic model based on DPAG score in two independent sets, the training set and the validation set. In both independent sets, GC samples were divided into low- and high-DPAG-score subgroups based on the optimal cutoff value of DPAG score (Fig. 8A and B). The clinical prognosis outcome indicated that in both independent sets, the survival outcome of GC samples in the low-DPAG-score subgroup was significantly better than that in the high-DPAG-score subgroup (Fig. 8C and D, $p < 0.001$). Additionally, in both sets, PCA based on DPAG prognostic features could accurately distinguish between the high- and low-DPAG-score subgroups (Fig. 8E and F). Based on these results, we conclude that the prognostic model based on DPAG score for predicting the survival outcome of GC is convincing and reliable.

Immune infiltration feature and drug sensitivity analysis in DPAG score subgroups

The ESTIMATE algorithm was used to investigate the immune status of GC samples with low and high DPAG scores. As shown in Supplementary Fig. 9A–D, GC samples with high DPAG scores had higher ESTIMATE, stromal, and immune scores, and lower tumor purity. Spearman correlation analysis revealed that the DPAG score was positively correlated with

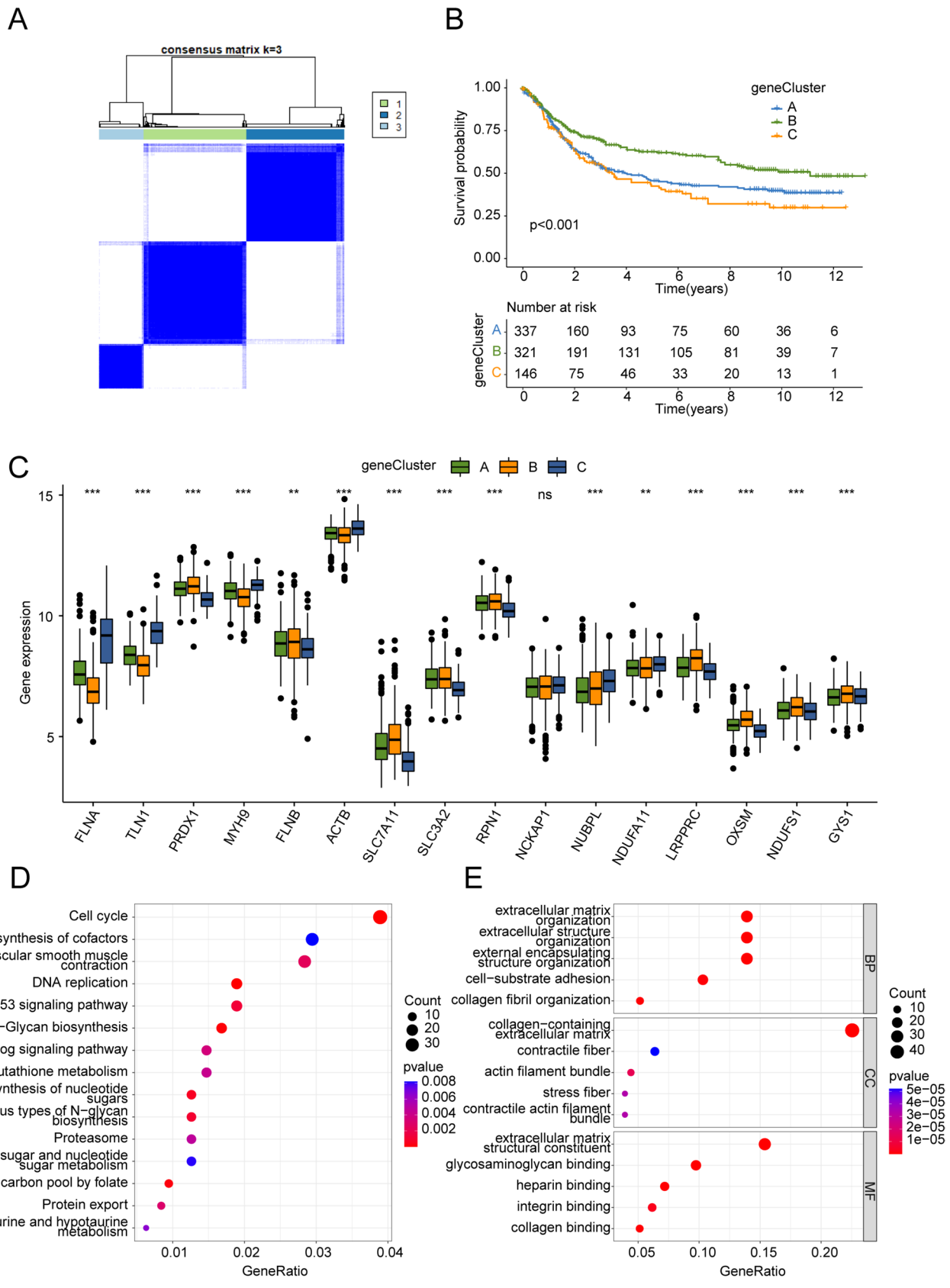
A
consensus matrix k=3
1
2
3
B
geneCluster
A
B
C
Survival probability
1.00
0.75
0.50
0.25
0.00
p<0.001
0
2
4
6
8
10
12
Time(years)
Number at risk
geneCluster
A 337 160 93 75 60 36 6
B 321 191 131 105 81 39 7
C 146 75 46 33 20 13 1
C
geneCluster A B C
Gene expression
15
10
5
ns
FLNA
TLN1
PRDX1
MYH9
FLNB
ACTB
SLC7A11
SLC3A2
RPN1
NCKAP1
NUBPL
NDUFA11
LRPPRC
OXSM
NDUFS1
GYS1
D
Cell cycle
Biosynthesis of cofactors
Vascular smooth muscle contraction
DNA replication
p53 signaling pathway
N−Glycan biosynthesis
Hedgehog signaling pathway
Glutathione metabolism
Biosynthesis of nucleotide sugars
Various types of N−glycan biosynthesis
Proteasome
Amino sugar and nucleotide sugar metabolism
One carbon pool by folate
Protein export
Taurine and hypotaurine metabolism
0.01
0.02
0.03
0.04
GeneRatio
Count
10
20
30
pvalue
0.008
0.006
0.004
0.002
E
extracellular matrix organization
extracellular structure organization
external encapsulating structure organization
cell−substrate adhesion
collagen fibril organization
collagen−containing extracellular matrix
contractile fiber
actin filament bundle
stress fiber
contractile actin filament bundle
extracellular matrix structural constituent
glycosaminoglycan binding
heparin binding
integrin binding
collagen binding
BP
CC
MF
0.05
0.10
0.15
0.20
GeneRatio
Count
10
20
30
40
pvalue
5e−05
4e−05
3e−05
2e−05
1e−05

◂**Fig. 4** Molecular subtypes generation based on the DPAG subtypes associated genes for GC. (**A**) Unsupervised consensus cluster analysis based on DPAG subtypes associated genes (k = 3). (**B**) Clinical survival prognosis analysis of GC in gene subtypes. (**C**) Differential expression analysis of 16 DPAGs in gene subtypes. (**D**, **E**) KEGG and GO enrichment analysis of DPAG subtype-associated genes. $*p < 0.05$, $**p < 0.01$, $***p < 0.001$, ns, no significance

mast cells, plasmacytoid dendritic cells, natural killer cells, natural killer T cells, immature dendritic cells, T follicular helper cells, regulatory T cells, type 1 T helper cells, and macrophages; but negatively correlated with $CD4^+$ T cells, neutrophils, CD8 + T cells, type 17 T helper cells, and type 2 T helper cells (Supplementary Fig. 9E). The ssGSEA results indicated a higher relative proportion of immune cells in the high-DPAG-scoring subgroup compared to the low-DPAG-scoring group (Supplementary Fig. 9F). Additionally, based on the GDSC database, a number of potential chemotherapeutic agents were predicted to be associated with the DPAG score. The drug sensitivity results showed that the IC50 for crizotinib, imatinib, and paclitaxel was significantly higher in the high-DPAG-score subgroup than in the low-DPAG-score subgroup, while the IC50 for dasatinib was significantly lower in the high-DPAG-score subgroup than in the low-DPAG-score subgroup (Supplementary Fig. 9G).

Immunotherapy response and somatic mutation feature in DPAG score subgroups

We further evaluated the immunotherapy response and somatic mutation characteristics of GC samples in different DPAG score subgroups. The IPS results suggested that the IPS score of the low-DPAG-score subgroup was significantly higher than that of the high-DPAG-score subgroup, indicating that GC samples in the low-DPAG-score subgroup may have a higher degree of responsiveness to CTLA4 and PD1 treatment strategies (Supplementary Fig. 10A–D). The MSI results showed that the DPAG score was lower in the H-MSI group than in the L-MSI and MSS groups, while the TMB results suggested that the TMB score was higher in the low-DPAG-score subgroup (Supplementary Fig. 10E and F). Survival curves indicated that in the subgroups of high TMB and low TMB, the clinical prognosis of GC samples in the low-DPAG-score group was significantly better than that in the high-DPAG-score subgroup (Supplementary Fig. 10G, $p < 0.001$). In the low-DPAG-score subgroup, we observed that out of 180 GC samples, 169 (93.89%) samples had somatic mutations, whereas in the high-DPAG-score subgroup, out of 182 samples, 147 (80.77%) samples had somatic mutations. It is worth noting that we found a significantly higher frequency of somatic mutations in the low-DPAG-score subgroup compared to the high-DPAG-score subgroup, such as TTN (low: 59% vs high: 34%), TP53 (low: 43% vs high: 40%), MUC16 (low: 40% vs high: 20%), ARID1A (low: 31% vs high: 16%), and LRP1B (low: 34% vs high: 14%) (Supplementary Fig. 10H and I).

Single-cell sequencing analysis reveals cell subpopulation and expression characteristics of DPAG prognostic signatures in GC

We further explored the classification of cell subpopulations and the distribution of DPAG signatures within these subpopulations at the single-cell sequencing level in GC. Based on the GC single-cell sequencing dataset GSE163558, we extracted single-cell sequencing data from three GC samples, performed quality control, and standardized processing for each sample (Supplementary Fig. 11A). Following normalization, 2000 highly variable genes were identified for subsequent PCA dimensionality reduction analysis (Supplementary Fig. 11B). Based on marker genes for different cell types, we accurately identified 22 cell types in the GC samples. The t-SNE and UMAP dimensionality reduction plots displayed the distribution patterns of these 22 cell types (Supplementary Fig. 11C and D). Violin plots indicated that most DPAG prognostic signatures, such as APC11, BRCC3, MED4, and SEC23A, were significantly expressed in the 22 cell types (Supplementary Fig. 11E). Using the SingleR annotation algorithm, we accurately identified 10 cell subpopulations in the GC samples: T cells, neutrophils, epithelial cells, monocytes, tissue stem cells, macrophages, B cells, NK cells, endothelial cells, and dendritic cells. The classification of these 10 subpopulations was visualized using t-SNE and UMAP plots (Supplementary Fig. 11F–H). Violin plots further revealed that the DPAG signatures were significantly expressed in all 10 cell subpopulations, with particularly high expression in T cells, neutrophils, epithelial cells, and monocytes (Supplementary Fig. 11I). By employing the UMAP dimensionality reduction algorithm, we demonstrated the localization and expression patterns of DPAG molecular subtype-related prognostic signatures across different cell subpopulations. Results showed that most DPAG prognostic signatures were highly expressed in epithelial cells, macrophages, and tissue stem cells (Supplementary Fig. 11J). These findings not only elucidate the composition of cell subpopulations in GC at the single-cell level but also further clarify the expression distribution of DPAG prognostic signatures within different cell subpopulations.

In vitro validation of the potential role of APC11 in GC

To validate the findings from our bioinformatics analysis, we conducted a series of experiments. First, we extracted RNA from normal gastric epithelial cells (GSE-1) and gastric cancer cells (AZ521, MKN45, MGC803) and

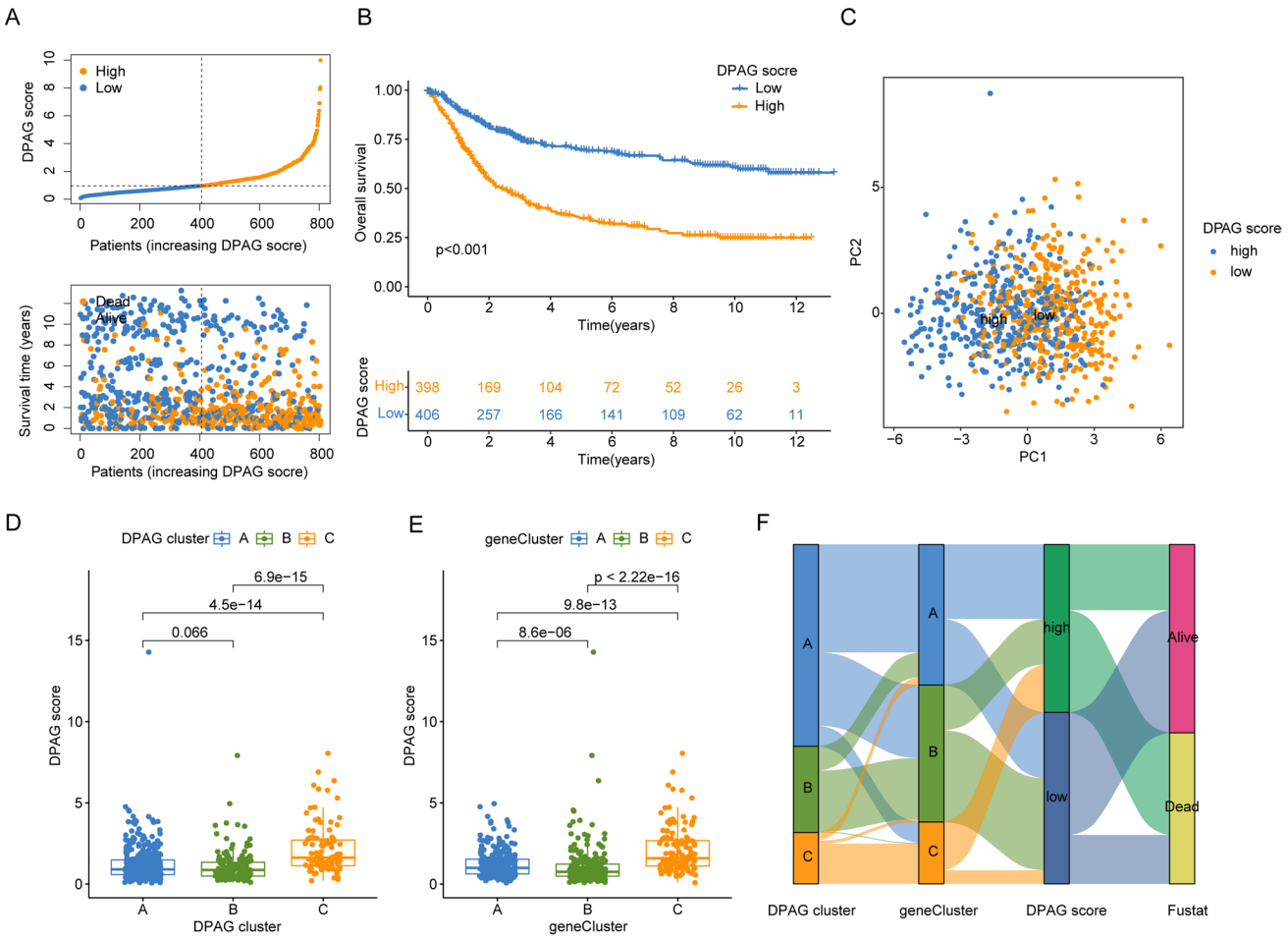

Fig. 5 Prognostic model development based on DPAG subtype-associated DEGs. (**A**) Division of high- and low-DPAG-score subgroups. (**B**) Clinical survival outcome analysis of DPAG score subgroups. (**C**) PCA analysis based on DPAG prognostic characteristics. (**D**) Distribution of DPAG scores in different DPAG subtypes. (**E**) Differential analysis of DPAG scores among different gene subtypes. (**F**) Potential association analysis of DPAG subtypes, gene subtypes, DPAG scores and survival outcomes of GC samples

measured the expression of APC11 using qRT-PCR. As shown in Supplementary Fig. 12A, APC11 expression was significantly higher in the cancer cells compared to the normal gastric epithelial cells. Similarly, Western blot analysis confirmed that APC11 protein levels were significantly elevated in gastric cancer cells compared to normal gastric epithelial cells (Supplementary Fig. 12B). Immunofluorescence staining also revealed that the fluorescence intensity of APC11 protein was higher in gastric cancer cells than in normal cells. Furthermore, we knocked down APC11 in gastric cancer cells using siRNA to clarify its function by examining the proliferation and migration of these cells (Supplementary Fig. 12C). The knockdown efficiency is shown in Supplementary Figs. 12D–F. The results of the CCK-8 assay indicated that APC11 knockdown significantly inhibited the proliferation of gastric cancer cells MGC803 (Fig. 1E) and AZ521 (Supplementary Fig. 12G). Additionally, colony formation ability was markedly reduced in both gastric cancer cell lines after APC11 knockdown (Supplementary Fig. 12H). Moreover, the Transwell assay demonstrated that the migratory capacity of MGC803 and AZ521 cells was significantly suppressed following APC11 knockdown. In summary, APC11 is highly expressed in gastric cancer, and its knockdown significantly inhibits the proliferation and migration of gastric cancer cells, highlighting its role as an oncogene.

Discussion

In this study, by establishing the characteristics of DPAG subtypes and analyzing their different-expressed genes, we defined DPAG score and proved that DPAG score is an independent prognostic factor significantly associated with GC

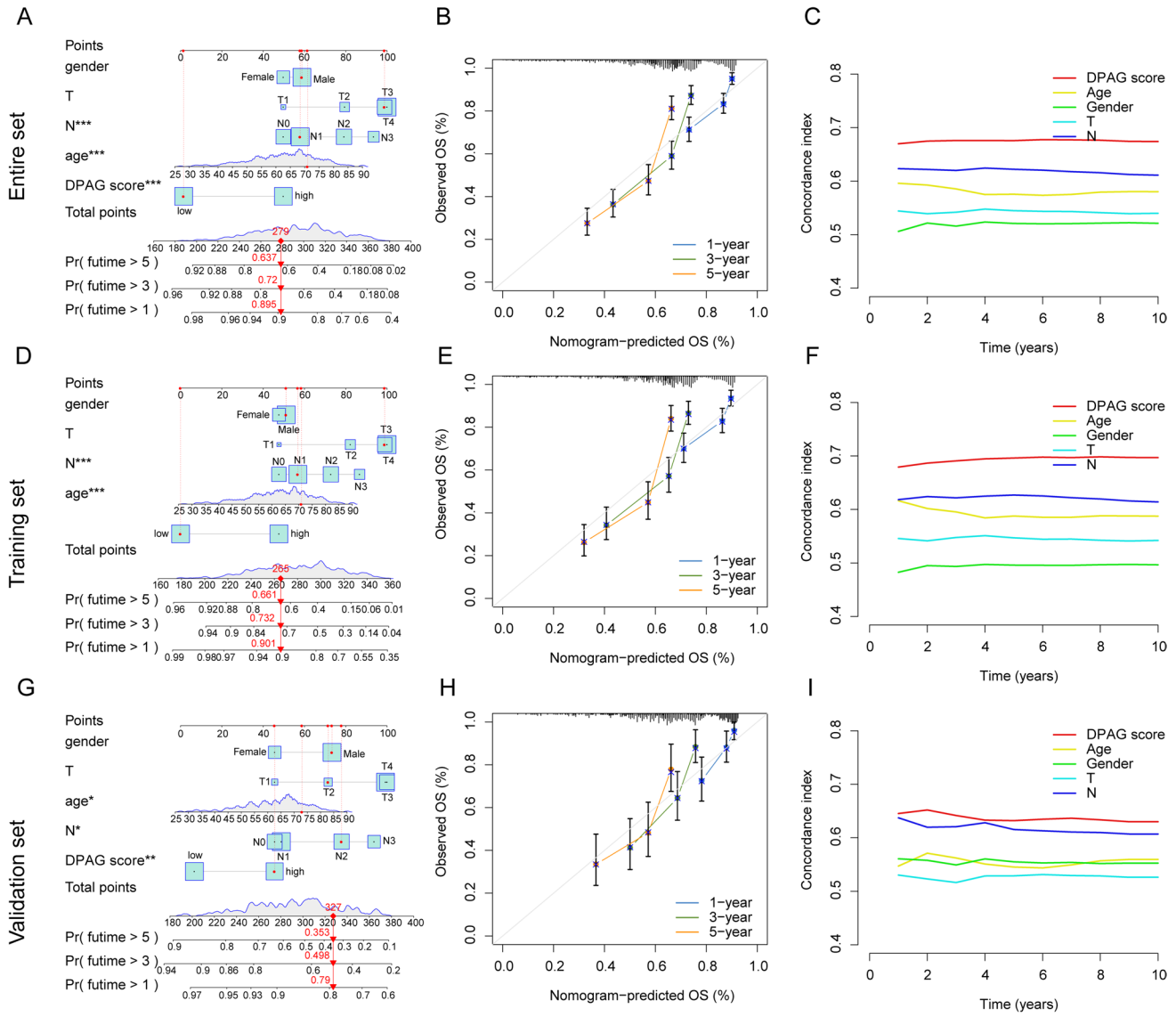

Fig. 6 Nomogram construction and C-index analysis of DPAG score in 3 independent sets. (**A**–**C**) Nomogram construction and C-index analysis based on DPAG score and clinical characteristics in the entire set. (**D**–**I**) Nomogram construction and C-index analysis in the training and validation sets

and poor prognosis of GC, indicating the important role of disulfidptosis in GC risk stratification.

Whether there is a disulfide stress in GC that causes disulfidptosis is not known. Excessive accumulation of cysteine is a key step in disulfide stress [6]. A Chinese cohort study found that serum concentrations of cysteine were associated with a significantly reduced risk of GC [25]. A Finnish study in men who smoked STAD showed a significant reduction in cysteine levels in STAD patients compared to healthy controls [26]. In addition, abnormal expression of cysteine dioxygenase 1 (CDO1), an enzyme that maintains cysteine homeostasis, can lead to cytotoxicity caused by elevated cysteine levels [27]. CDO1 expression is decreased in GC tissues and is an independent prognostic marker [28, 29]. This evidence suggests that disulfidptosis may play a role in GC progression.

Through bioinformatics analysis and in vitro experiments, we gave the first evidence that APC11 acts as an oncogene in GC. APC11 is associated with cyclin ubiquitination and participates in the formation of the E3 ligase complex [30, 31]. Knockdown of APC11 results in decreased cell cycle distribution in G2/M phase [32]. By regulating the ubiquitination degradation of key cyclins during tumor cell proliferation, APC11 can participate in the growth of a variety of tumors, including non-small cell lung cancer, colorectal cancer, and urothelial bladder cancer [33–35]. Overexpression of APC11 may predict a poor prognosis in tumor patients [36]. For the first time, we present evidence for APC11 in

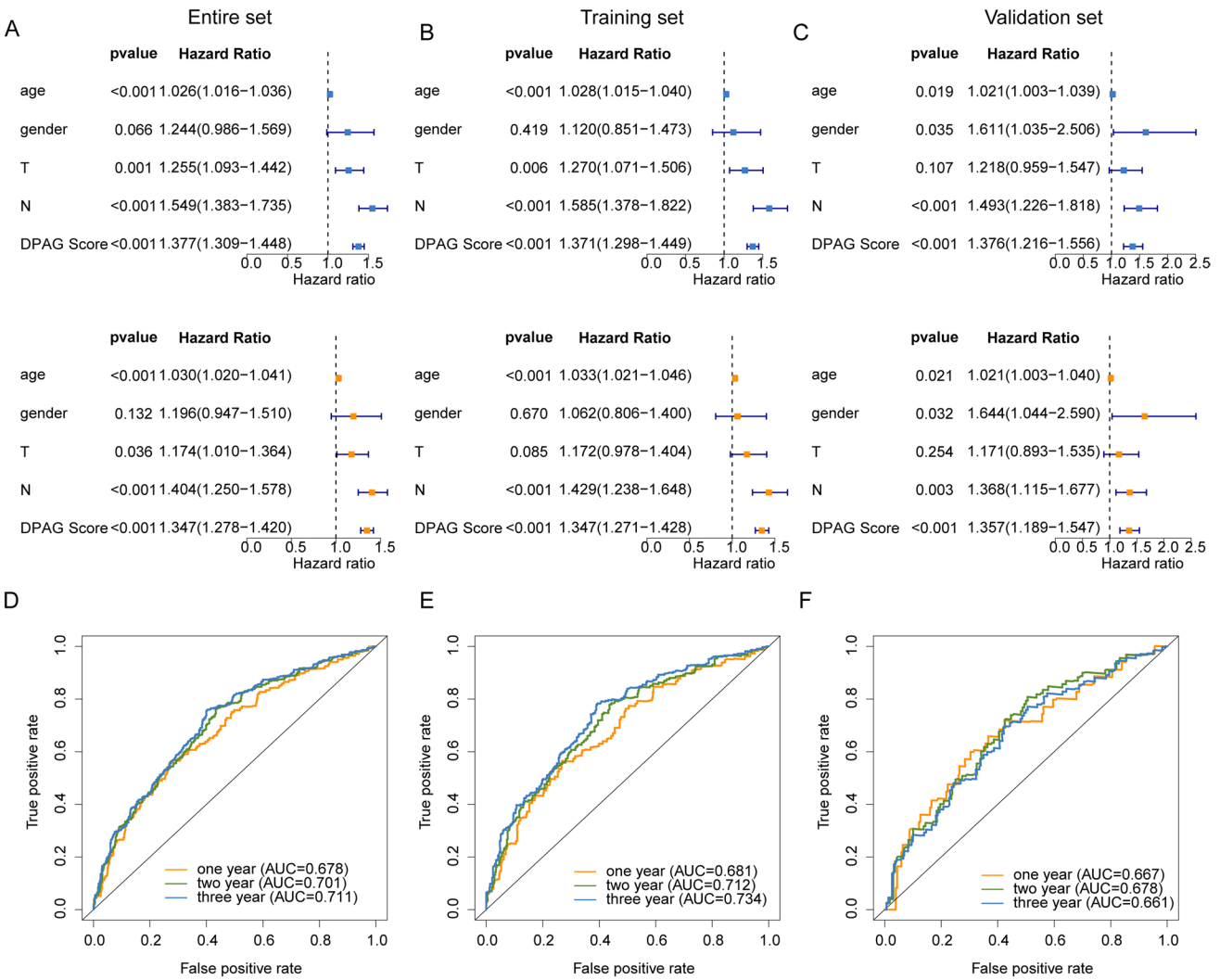

Fig. 7 Independence evaluation of DPAG score and clinical features in 3 independent sets. (**A**–**C**) Univariate and multivariate Cox analysis of DPAG score and clinical characteristics in entire, training and validation sets. (**D**–**F**) Time-associated ROC curve shows the AUC of 1, 3, and 5 years in the 3 independent sets

GC as oncogene, which is of positive significance to further reveal its mechanism.

Drug sensitivity tests showed differences in sensitivity of drugs such as paclitaxel in patients with different risk stratification. The FLOT regimen containing docetaxel has become the LAGC standard for perioperative chemotherapy in European countries [37, 38]. In China, among advanced gastric cancer patients who could not tolerate SOX first-line neoadjuvant chemotherapy regimen, paclitaxel chemotherapy regimen showed satisfactory efficacy and safety in treatment [39, 40]. Paclitaxel has also been used as a perioperative chemotherapy regimen for patients with locally advanced resectable GC [41]. However, limitations in the efficacy of paclitaxel have also been reported [42]. This study provides a new perspective and evidence for the prediction of the efficacy of paclitaxel in GC.

Our results show that plasmacytoid dendritic cells (pDC) expression is significantly increased in patients with high DPAG scores and is associated with a poorer prognosis. One of the main functions of pDC is to produce IFN and plays a crucial role in antiviral activity [43]. However, there is growing evidence that in the tumor-associated immune microenvironment, pDC can be hijacked and unable to produce IFN required for anti-tumor processes [44]. In addition, pDC may further develop and maintain an inhibitory immune environment in the tumor microenvironment [45, 46]. Our results also suggest a correlation between pDC and the immunosuppressive microenvironment. Immune activation strategies targeting pDC, such as TLR agonists, can reprogram pDC and reinduce tumor rejection in the clinical setting [44]. Although the research

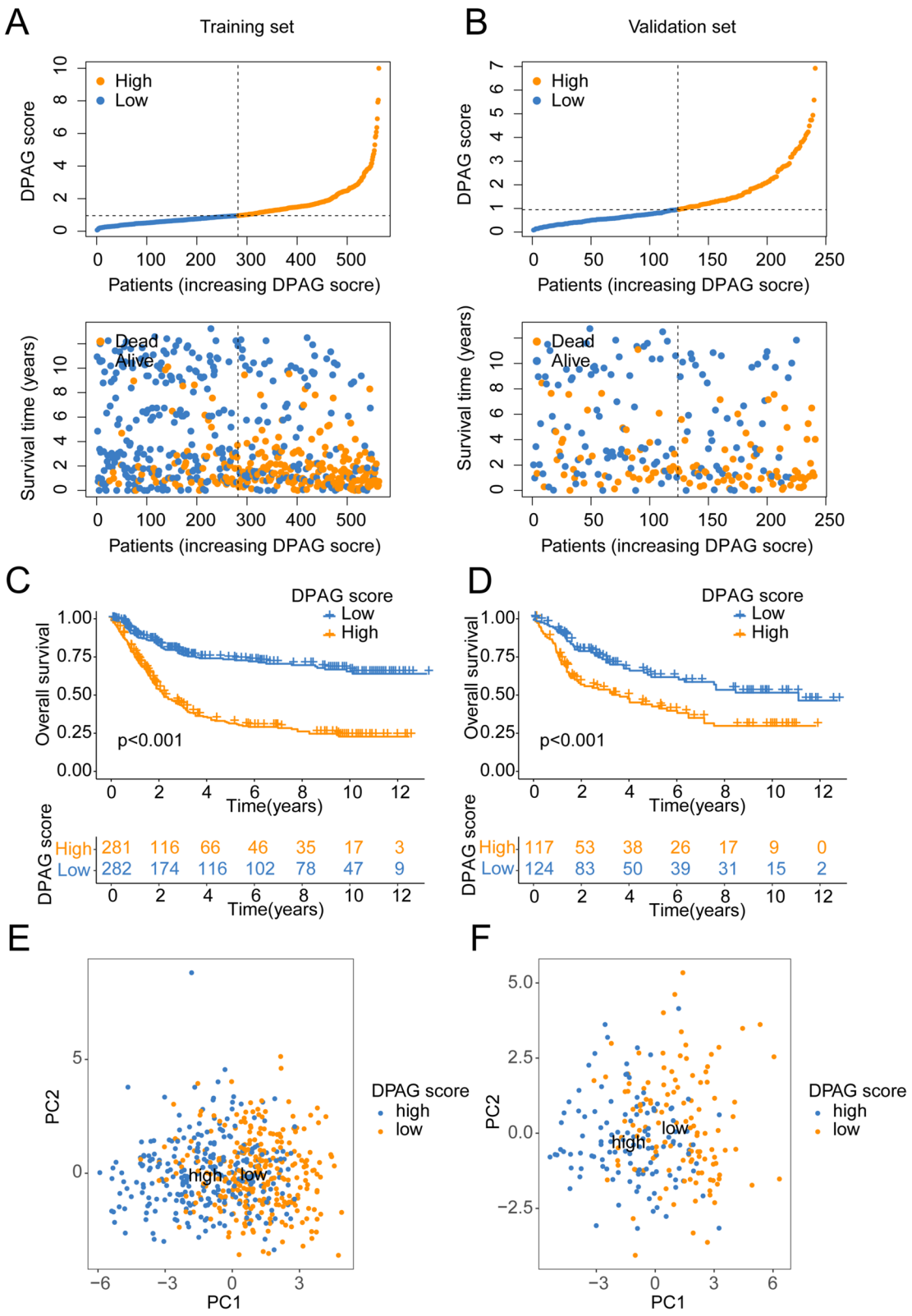

Fig. 8 Prognosis model development of DPAG score in the training and validation sets. (**A**, **B**) Division of low- and high-DPAG-score subgroups in the training and validation sets. (**C**, **D**) Clinical survival outcome analysis of low- and high-DPAG-score subgroups. (**E**, **F**) Unsupervised PCA plot of high- and low-DPAG-score subgroups in the training and validation sets

in GC is not comprehensive, further research on pDC has potential value for clinical application.

The extracellular matrix (ECM) related pathways are highly enriched in DPAG subcomponent differential genes. Changes in the microenvironment caused by ECM remodeling can lead to cancer progression and metastasis [47]. The content of ECM in normal gastric tissues is significantly different from that in GC, suggesting the potential of ECM as a novel diagnostic and prognostic biomarker for GC [48, 49]. In addition to its prognostic value [50], regulation of ECM-related genes can promote GC cell growth and migration [51]. Our results show the correlation between GC prognostic differences and ECM-related pathways, and also suggest the important value of ECM in risk stratification of gastric cancer.

Advances in single-cell sequencing technology enable deeper analysis of tumorigenesis, tumor progression, TME heterogeneity, and multi-dimensional individualized therapy at single-cell resolution [52–54]. Both the complexity and heterogeneity of GC are better explained through single-cell sequencing [55]. In this study, we further elucidated the expression distribution of DPAG prognostic features in different cell subsets through single-cell sequencing, indicating the important role of single-cell sequencing in GC. In fact, the characterization of inflammatory infiltration at different stages of GC by single-cell sequencing contributes to the identification of personalized treatment options for different stages of GC [55]. It is of positive significance to further overcome the limitations of single-cell sequencing in application.

Although we successfully verified the predictive value of DPAG score for GC prognosis and selected potential intervention targets, we failed to conduct further in vitro experimental analysis of the signaling pathways or molecular mechanisms related to the influence of DPAG score on GC prognosis. The specific regulatory processes of disulfidptosis still need further verification. In addition, the conclusion of correlation obtained by bioinformatics analysis also requires further causality verification. Therefore, the clinical application potential of DPAG score needs to be further explored. Further studies of disulfidptosis and DPAG scores in future will help deepen our understanding of the pathogenesis of GC.

Supplementary Information The online version contains supplementary material available at https://doi.org/10.1007/s00262-024-03883-3.

Author contributions HZ conceived and designed the study. QL and ZW contributed the data collection and data analysis. YL and SZ conceived the original ideas and finished the experiment section of this manuscript. JH and YL contributed the table and figures of this manuscript. YL, HZ, and JH contributed equally to this article and all authors contributed to the article and approved the submitted version.

Funding This study was supported by Zhejiang Province Health and Medicine Science and Technology Program (No. 2023KY615) and Science and Technology Program of Traditional Chinese Medicine in Zhejiang Province (No. 2023ZR066).

Data availability All data generated or analyzed during this study are included in this published article and its supplementary information files.

Declarations

Conflict of interests The authors declare no competing interests.

References

1. Sung H, Ferlay J, Siegel RL, Laversanne M, Soerjomataram I, Jemal A, Bray F (2021) Global cancer statistics 2020: GLOBOCAN estimates of incidence and mortality worldwide for 36 cancers in 185 countries. CA Cancer J Clin 71(3):209–249
2. Niclauss N, Gutgemann I, Dohmen J, Kalff JC, Lingohr P (2021) Novel biomarkers of gastric adenocarcinoma: current research and future perspectives. Cancers (Basel) 13(22):5660
3. Hirata Y, Noorani A, Song S, Wang L, Ajani JA (2023) Early stage gastric adenocarcinoma: clinical and molecular landscapes. Nat Rev Clin Oncol 20(7):453–469
4. Huang RJ, Laszkowska M, In H, Hwang JH, Epplein M (2023) Controlling gastric cancer in a world of heterogeneous risk. Gastroenterology 164(5):736–751
5. Liu X, Nie L, Zhang Y, Yan Y, Wang C, Colic M, Olszewski K, Horbath A, Chen X, Lei G et al (2023) Actin cytoskeleton vulnerability to disulfide stress mediates disulfidptosis. Nat Cell Biol 25(3):404–414
6. Koppula P, Zhuang L, Gan B (2021) Cystine transporter SLC7A11/xCT in cancer: ferroptosis, nutrient dependency, and cancer therapy. Protein Cell 12(8):599–620
7. Machesky LM (2023) Deadly actin collapse by disulfidptosis. Nat Cell Biol 25(3):375–376
8. Yan Y, Teng H, Hang Q, Kondiparthi L, Lei G, Horbath A, Liu X, Mao C, Wu S, Zhuang L et al (2023) SLC7A11 expression level dictates differential responses to oxidative stress in cancer cells. Nat Commun 14(1):3673
9. Mao SH, Zhu CH, Nie Y, Yu J, Wang L (2021) Levobupivacaine induces ferroptosis by miR-489-3p/SLC7A11 signaling in gastric cancer. Front Pharmacol 12:681338

10. Chen L, Qiao L, Bian Y, Sun X (2020) GDF15 knockdown promotes erastin-induced ferroptosis by decreasing SLC7A11 expression. Biochem Biophys Res Commun 526(2):293–299
11. Lin Z, Song J, Gao Y, Huang S, Dou R, Zhong P, Xiong B (2022) Hypoxia-induced HIF-1α/lncRNA-PMAN inhibits ferroptosis by promoting the cytoplasmic translocation of ELAVL1 in peritoneal dissemination from gastric cancer. Redox Biol 52:102312
12. Liu J, Yang H, Deng J, Jiang R, Meng E, Wu H (2023) CircRPPH1 promotes the stemness of gastric cancer cells by targeting miR-375/SLC7A11 axis. Environ Toxicol 38(1):115–125
13. Lakatos E, Williams MJ, Schenck RO, Cross WCH, Househam J, Zapata L, Werner B, Gatenbee C, Robertson-Tessi M, Barnes CP et al (2020) Evolutionary dynamics of neoantigens in growing tumors. Nat Genet 52(10):1057–1066
14. Cai L, Li L, Ren D, Song X, Mao B, Han B, Zhang H (2020) Prognostic impact of gene copy number instability and tumor mutation burden in patients with resectable gastric cancer. Cancer Commun (Lond) 40(1):63–66
15. Zhang P, Liu M, Cui Y, Zheng P, Liu Y (2021) Microsatellite instability status differentially associates with intratumoral immune microenvironment in human cancers. Brief Bioinform 22(3)
16. He J, Ding H, Li H, Pan Z, Chen Q (2021) Intra-tumoral expression of SLC7A11 is associated with immune microenvironment, drug resistance, and prognosis in cancers: a pan-cancer analysis. Front Genet 12:770857
17. Mou P, Ge QH, Sheng R, Zhu TF, Liu Y, Ding K (2023) Research progress on the immune microenvironment and immunotherapy in gastric cancer. Front Immunol 14:1291117
18. Wang B, Xu D, Yu X, Ding T, Rao H, Zhan Y, Zheng L, Li L (2011) Association of intra-tumoral infiltrating macrophages and regulatory T cells is an independent prognostic factor in gastric cancer after radical resection. Ann Surg Oncol 18(9):2585–2593
19. Cristescu R, Lee J, Nebozhyn M, Kim KM, Ting JC, Wong SS, Liu J, Yue YG, Wang J, Yu K et al (2015) Molecular analysis of gastric cancer identifies subtypes associated with distinct clinical outcomes. Nat Med 21(5):449–456
20. Shikuma J, Nagai Y, Sakurai M, Udagawa K, Ito R, Miwa T, Suzuki R (2022) Impact of gender differences on lifestyle and glycemic control in Japanese patients with diabetes during COVID-19 lockdowns. Prim Care Diabetes
21. Hinshaw DC, Shevde LA (2019) The tumor microenvironment innately modulates cancer progression. Cancer Res 79(18):4557–4566
22. Lei X, Lei Y, Li JK, Du WX, Li RG, Yang J, Li J, Li F, Tan HB (2020) Immune cells within the tumor microenvironment: Biological functions and roles in cancer immunotherapy. Cancer Lett 470:126–133
23. Leek JT, Johnson WE, Parker HS, Jaffe AE, Storey JD (2012) The sva package for removing batch effects and other unwanted variation in high-throughput experiments. Bioinformatics 28(6):882–883
24. Liu X, Nie L, Zhang Y, Yan Y, Wang C, Colic M, Gan B (2023) Actin cytoskeleton vulnerability to disulfide stress mediates disulfidptosis. Nat Cell Biol 25(3):404–414
25. Murphy G, Fan JH, Mark SD, Dawsey SM, Selhub J, Wang J, Taylor PR, Qiao YL, Abnet CC (2011) Prospective study of serum cysteine levels and oesophageal and gastric cancers in China. Gut 60(5):618–623
26. Miranti EH, Freedman ND, Weinstein SJ, Abnet CC, Selhub J, Murphy G, Diaw L, Mannisto S, Taylor PR, Albanes D et al (2016) Prospective study of serum cysteine and cysteinylglycine and cancer of the head and neck, esophagus, and stomach in a cohort of male smokers. Am J Clin Nutr 104(3):686–693
27. Stipanuk MH, Ueki I, Dominy JE Jr, Simmons CR, Hirschberger LL (2009) Cysteine dioxygenase: a robust system for regulation of cellular cysteine levels. Amino Acids 37(1):55–63
28. Ma G, Zhao Z, Qu Y, Cai F, Liu S, Liang H, Zhang R, Deng J (2022) Cysteine dioxygenase 1 attenuates the proliferation via inducing oxidative stress and integrated stress response in gastric cancer cells. Cell Death Discov 8(1):493
29. Hao S, Yu J, He W, Huang Q, Zhao Y, Liang B, Zhang S, Wen Z, Dong S, Rao J et al (2017) Cysteine dioxygenase 1 mediates erastin-induced ferroptosis in human gastric cancer cells. Neoplasia 19(12):1022–1032
30. Tang Z, Li B, Bharadwaj R, Zhu H, Ozkan E, Hakala K, Deisenhofer J, Yu H (2001) APC2 Cullin protein and APC11 RING protein comprise the minimal ubiquitin ligase module of the anaphase-promoting complex. Mol Biol Cell 12(12):3839–3851
31. Kelly A, Wickliffe KE, Song L, Fedrigo I, Rape M (2014) Ubiquitin chain elongation requires E3-dependent tracking of the emerging conjugate. Mol Cell 56(2):232–245
32. Shi YJ, Huo KK (2012) Knockdown expression of Apc11 leads to cell-cycle distribution reduction in G2/M phase. Genet Mol Res 11(3):2814–2822
33. Drouet Y, Treilleux I, Viari A, Leon S, Devouassoux-Shisheboran M, Voirin N, de la Fouchardiere C, Manship B, Puisieux A, Lasset C et al (2018) Integrated analysis highlights APC11 protein expression as a likely new independent predictive marker for colorectal cancer. Sci Rep 8(1):7386
34. Wang F, Chen X, Yu X, Lin Q (2019) Degradation of CCNB1 mediated by APC11 through UBA52 ubiquitination promotes cell cycle progression and proliferation of non-small cell lung cancer cells. Am J Transl Res 11(11):7166–7185
35. Yan D, He Q, Pei L, Yang M, Huang L, Kong J, He W, Liu H, Xu S, Qin H et al (2023) The APC/C E3 ligase subunit ANAPC11 mediates FOXO3 protein degradation to promote cell proliferation and lymph node metastasis in urothelial bladder cancer. Cell Death Dis 14(8):516
36. Zhou J, Zhang S, Fu G, He Z, Xu Y, Ye W, Chen Z (2018) Overexpression of APC11 predicts worse survival in lung adenocarcinoma. Onco Targets Ther 11:7125–7132
37. Al-Batran SE, Hofheinz RD, Pauligk C, Kopp HG, Haag GM, Luley KB, Meiler J, Homann N, Lorenzen S, Schmalenberg H et al (2016) Histopathological regression after neoadjuvant docetaxel, oxaliplatin, fluorouracil, and leucovorin versus epirubicin, cisplatin, and fluorouracil or capecitabine in patients with resectable gastric or gastro-oesophageal junction adenocarcinoma (FLOT4-AIO): results from the phase 2 part of a multicentre, open-label, randomised phase 2/3 trial. Lancet Oncol 17(12):1697–1708
38. Al-Batran SE, Homann N, Pauligk C, Goetze TO, Meiler J, Kasper S, Kopp HG, Mayer F, Haag GM, Luley K et al (2019) Perioperative chemotherapy with fluorouracil plus leucovorin, oxaliplatin, and docetaxel versus fluorouracil or capecitabine plus cisplatin and epirubicin for locally advanced, resectable gastric or gastro-oesophageal junction adenocarcinoma (FLOT4): a randomised, phase 2/3 trial. Lancet 393(10184):1948–1957
39. Lu Z, Zhang X, Liu W, Liu T, Hu B, Li W, Fan Q, Xu J, Xu N, Bai Y et al (2018) A multicenter, randomized trial comparing efficacy and safety of paclitaxel/capecitabine and cisplatin/capecitabine in advanced gastric cancer. Gastric Cancer 21(5):782–791
40. Yeh KH, Lu YS, Hsu CH, Lin JF, Hsu C, Kuo SH, Li SJ, Cheng AL (2005) Phase II study of weekly paclitaxel and 24-hour infusion of high-dose 5-fluorouracil and leucovorin in the treatment of recurrent or metastatic gastric cancer. Oncology 69(1):88–95
41. Sah BK, Zhang B, Zhang H, Li J, Yuan F, Ma T, Shi M, Xu W, Zhu Z, Liu W et al (2020) Neoadjuvant FLOT versus SOX phase II randomized clinical trial for patients with locally advanced gastric cancer. Nat Commun 11(1):6093

42. Suh KJ, Ryu MH, Zang DY, Bae WK, Lee HS, Oh HJ, Lee KW (2023) AZD8186 in combination with paclitaxel in patients with advanced gastric cancer: results from a phase Ib/II study (KCSG ST18-20). Oncologist 28(9):e823–e834
43. Yu H, Mei Y, Dong Y, Chen C, Lin X, Jin H, Yu J, Liu X (2023) CCR9-CCL25 mediated plasmacytoid dendritic cell homing and contributed the immunosuppressive microenvironment in gastric cancer. Transl Oncol 33:101682
44. Vermi W, Soncini M, Melocchi L, Sozzani S, Facchetti F (2011) Plasmacytoid dendritic cells and cancer. J Leukoc Biol 90(4):681–690
45. Demoulin S, Herfs M, Delvenne P, Hubert P (2013) Tumor microenvironment converts plasmacytoid dendritic cells into immunosuppressive/tolerogenic cells: insight into the molecular mechanisms. J Leukoc Biol 93(3):343–352
46. Yu H, Huang X, Liu X, Jin H, Zhang G, Zhang Q, Yu J (2013) Regulatory T cells and plasmacytoid dendritic cells contribute to the immune escape of papillary thyroid cancer coexisting with multinodular non-toxic goiter. Endocrine 44(1):172–181
47. Winkler J, Abisoye-Ogunniyan A, Metcalf KJ, Werb Z (2020) Concepts of extracellular matrix remodelling in tumour progression and metastasis. Nat Commun 11(1):5120
48. Moreira AM, Ferreira RM, Carneiro P, Figueiredo J, Osorio H, Barbosa J, Preto J, Pinto-do OP, Carneiro F, Seruca R (2022) Proteomic identification of a gastric tumor ECM signature associated with cancer progression. Front Mol Biosci 9:818552
49. Theocharis AD, Vynios DH, Papageorgakopoulou N, Skandalis SS, Theocharis DA (2003) Altered content composition and structure of glycosaminoglycans and proteoglycans in gastric carcinoma. Int J Biochem Cell Biol 35(3):376–390
50. Jiang K, Liu H, Xie D, Xiao Q (2019) Differentially expressed genes ASPN, COL1A1, FN1, VCAN and MUC5AC are potential prognostic biomarkers for gastric cancer. Oncol Lett 17(3):3191–3202
51. Liu C, Deng L, Lin J, Zhang J, Huang S, Zhao J, Jin P, Xu P, Ni P, Xu D et al (2020) Zinc finger protein CTCF regulates extracellular matrix (ECM)-related gene expression associated with the Wnt signaling pathway in gastric cancer. Front Oncol 10:625633
52. Tsubosaka A, Komura D, Kakiuchi M, Katoh H, Onoyama T, Yamamoto A, Abe H, Seto Y, Ushiku T, Ishikawa S (2023) Stomach encyclopedia: combined single-cell and spatial transcriptomics reveal cell diversity and homeostatic regulation of human stomach. Cell Rep 42(10):113236
53. Sun C, Wang A, Zhou Y, Chen P, Wang X, Huang J, Gao J, Wang X, Shu L, Lu J et al (2023) Spatially resolved multi-omics highlights cell-specific metabolic remodeling and interactions in gastric cancer. Nat Commun 14(1):2692
54. Chang R, Tsui KH, Pan LF, Li CJ (2024) Spatial and single-cell analyses uncover links between ALKBH1 and tumor-associated macrophages in gastric cancer. Cancer Cell Int 24(1):57
55. Xu J, Yu B, Wang F, Yang J (2024) Single-cell RNA sequencing to map tumor heterogeneity in gastric carcinogenesis paving roads to individualized therapy. Cancer Immunol Immunother 73(11):233